A New Use for a Familiar Fold: The X-ray Crystal Structure of GTP-Bound GTP Cyclohydrolase III from *Methanocaldococcus jannaschii* Reveals a Two Metal Ion Catalytic Mechanism[†,‡]

Shane D. Morrison,[§] Sue A. Roberts,[§] Abreeza M. Zegeer,[§] William R. Montfort,[§,||] and Vahe Bandarian*[,§,||]

Department of Biochemistry and Molecular Biophysics and Department of Chemistry, The University of Arizona, Tucson, Arizona 85721

Received August 30, 2007; Revised Manuscript Received October 26, 2007

ABSTRACT: GTP cyclohydrolase (GCH) III from *Methanocaldococcus jannaschii*, which catalyzes the conversion of GTP to 2-amino-5-formylamino-6-ribosylamino-4(3*H*)-pyrimidinone 5′-phosphate (FAPy), has been shown to require Mg^{2+} for catalytic activity and is activated by monovalent cations such as K^+ and ammonium [Graham, D. E., Xu, H., and White, R. H. (2002) *Biochemistry 41*, 15074−15084]. The reaction is formally identical to that catalyzed by a GCH II ortholog (SCO 6655) from *Streptomyces coelicolor*; however, SCO 6655, like other GCH II proteins, is a zinc-containing protein. The structure of GCH III complexed with GTP solved at 2 Å resolution clearly shows that GCH III adopts a distinct fold that is closely related to the palm domains of phosphodiesterases, such as DNA polymerase I. GCH III is a tetramer of identical subunits; each monomer is composed of an N- and a C-terminal domain that adopt nearly superimposible structures, suggesting that the protein has arisen by gene duplication. Three metal ions were located in the active site, two of which occupy positions that are analogous to those occupied by divalent metal ions in the structures of a number of palm domain containing proteins, such as DNA polymerase I. Two conserved Asp residues that coordinate the metal ions, which are also found in palm domain containing proteins, are observed in GCH III. Site-directed variants (Asp→Asn) of these residues in GCH III are less active than wild-type. The third metal ion, most likely a potassium ion, is involved in substrate recognition through coordination of O6 of GTP. The arrangement of the metal ions in the active site suggests that GCH III utilizes two metal ion catalysis. The structure of GCH III extends the repertoire of possible reactions with a palm fold to include cyclohydrolase chemistry.

GTP[1] is a common biosynthetic starting point for a large array of purine-based biologically important molecules, including folic acid and riboflavin, which are required for processes as diverse as one-carbon metabolism and circadian rhythm. The overall pathways that give rise to these metabolites vary substantially; however, the first step in the pathway to each is catalyzed by a GTP cyclohydrolase (GCH), and the hydrolysis of the linkage between C-8 of GTP and N-9 is a common step. Intriguingly, despite the similarities in the chemical transformations that are required for these biosynthetic pathways, all evidence to date points to involvement of structurally distinct enzymes for this step. However, the structural landscape of the enzymes involved in these steps is not complete.

Four classes of GCH proteins have been described (Figure 1). GCH I catalyzes the first step in the biosynthesis of folic acid, which is conversion of GTP to dihydroneopterin triphosphate (*1*, *2*). GCH II catalyzes the first step in the biosynthesis of flavocoenzymes, which entails conversion of GTP to 2,5-diamino-6-ribosylamino-4(3*H*)-pyrimidinone 5′-phosphate (APy) (*3*, *4*). GCH III catalyzes the conversion of GTP to 2-amino-5-formylamino-6-ribosylamino-4(3*H*)-pyrimidinone 5′-phosphate (FAPy) (*5*); the physiological function of this protein is not known, though it may be involved in the biosynthesis of riboflavin and coenzyme F_{420}. The fourth GCH class is represented by MptA, which catalyzes the conversion of GTP to 7,8-dihydro-D-neopterin 2′,3′-cyclic phosphate, an early intermediate to pterins in archaea (*6*). X-ray crystal structures of GCH I and II have been solved showing that these proteins adopt distinct folds. Structures of GCH III and MptA, which are predicted to adopt different folds by bioinformatics analysis, have not been available.

[†] Support from National Institutes of Health grants GM72623 (to V.B.) and HL62969 (to W.R.M.) is gratefully acknowledged. In addition, the research of V.B. is supported (in part) by a Career Award in Biomedical Sciences from the Burroughs Wellcome Fund. S.D.M was partially funded by Howard Hughes Medical Institute (grant 52003749). The SSRL Structural Molecular Biology Program is supported by the Department of Energy, Office of Biological and Environmental Research, and by the National Institutes of Health, National Center for Research Resources, Biomedical Technology Program, and the National Institute of General Medical Sciences.

[‡] Coordinates and structure factors have been deposited in the Protein Data Bank (PDB entry 2QV6)

* Corresponding author. Phone: (520) 626-0389. Fax: (520) 621-1697. E-mail: vahe@email.arizona.edu.

[§] Department of Biochemistry and Molecular Biophysics.

[||] Department of Chemistry.

[1] Abbreviations: APy, 2,5-diamino-6-ribosylamino-4(3*H*)-pyrimidinone 5′-phosphate; GCH, GTP cyclohydrolase; GTP, guanosine 5′-triphosphate; FAPy, 2-amino-5-formylamino-6-ribosylamino-4(3*H*)-pyrimidinone 5′-phosphate; Tris, 2-amino-2-(hydroxymethyl)propane-1,3-diol.

10.1021/bi701782e CCC: $40.75
Published on Web 12/04/2007

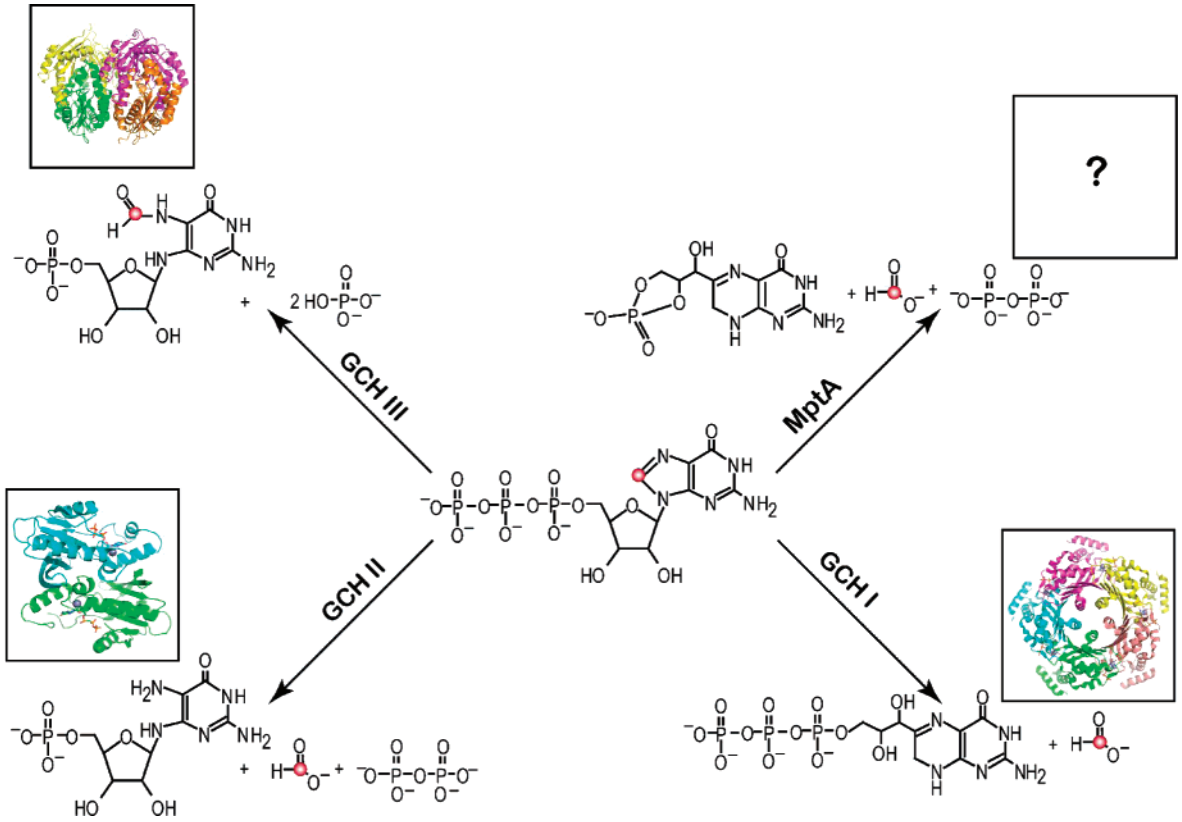

FIGURE 1: Reactions catalyzed by GTP cyclohydrolases. Structures of GCH I (1WUR) and GCH II (2BZ0) are shown in cartoon representation to illustrate differing folds. GCH I is a dimer of pentamers that is associated in two toroids in a T-fold (*52*, *53*). GCH II is a dimer that adopts an $\alpha-\beta$ fold (*12*). The GCH III structure shown is described in this paper.

We have recently characterized a GTP cyclohydrolase II ortholog (SCO 6655) from *Streptomyces coelicolor* that, based on sequence analysis, appears to be structurally related to GCH II (*7*); however, this protein catalyzes the conversion of GTP to FAPy, instead of to APy. Site-directed mutagenesis studies have shown that the GTP→FAPy activity appears to result from a single amino acid substitution in this protein, whereby a Tyr residue in the active site has been changed to a Met (*7*). Additional biochemical studies have shown that interchange of this residue in this protein or other GCH II homologs that catalyze the conversion of GTP to APy is sufficient to change the identity of the product that is formed; the presence of Tyr leads to formation of APy and a Met promotes formation of FAPy (J. E. Spoonamore, V. Bandarian, unpublished observations).

GCH III is a protein from *Methanocaldococcus jannaschii* that catalyzes a reaction that is formally similar to that of SCO6655 (GTP→FAPy). However, biochemical studies have shown that unlike GCH I and II, which are zinc-containing proteins (*8*−*12*), GCH III requires Mg^{2+} and is activated by large monovalent cations, such as potassium or ammonium (*5*). GCH III is not related to any other proteins in the NCBI database besides a family of archea proteins (Pfam05165) that share a conserved GGDN motif. Indeed, GCH III is unique to archaea and has been identified as part of an archaeal genomic signature (*13*). Biochemical data support the notion that GCH III may be utilizing a new mechanism, one not requiring Zn^{2+}, for hydrolysis of the C-8−N-9 bond of GTP.

The dearth of structural information on the archaeal proteins, MptA and GCH III, hampers efforts to explore the evolutionary relationships between these proteins and GTP cyclohydrolases. In this paper, we report the 2.0 Å resolution X-ray crystal structure of GCH III from *M. jannaschii* (MJ0145) bound to its substrate GTP. GCH III is structurally unlike any known GCH protein. Aside from revealing a new fold involved in GTP cyclohydrolase chemistry, the GTP-bound structure also reveals three metal ions bound to GTP and the protein, two of which almost certainly play mechanistic roles analogous to those involved in two metal ion catalysis by nucleotide modification enzymes, such as DNA polymerase I. In fact, structural comparisons illustrate that the binding sites for the two metal ions overlap in each protein. Not only is GCH III structurally and mechanistically distinct from GCH I and GCH II but it has common ancestry with DNA polymerase, adenylyl cyclase, and other palm domain containing proteins.

EXPERIMENTAL PROCEDURES

Materials. Genomic DNA for *M. jannaschii* was obtained from American Type Culture Collection (43067D). The vectors pGEM Easy-T, pET28a, and pET29a were obtained from Promega and Novagen, respectively. Pfu DNA polymerase was from Stratagene and deoxynucleotides were from Invitrogen. The cell lines XL1-Blue and BL21(DE3) were obtained from Stratagene and Novagen. The restriction enzymes *Nde*I and *Hin*dIII were from New England Biolabs. LB medium refers to Lenox broth. 2-Amino-2-(hydroxymethyl)propane-1,3-diol (Tris) was from EMD Sciences. The Q-Sepharose (fast flow) and Butyl Sepharose 4 (fast flow) resins that were used for purifications were from Amersham Biosciences. PMSF was obtained from EM Sciences. Gua-

Table 1: Primers Used in Cloning and Mutagenesis of MJ0145

open reading frame	primer	sequence[a]
MJ0145	VBD249	5′-GGAAGAGATGGGAAACAT*ATG*ATT CAAATAACAGTAATTCAGATAG-3′
	VBD250	5′-CTATAAAATCACAAGC*TTATT* *A*AAACTGTGGATGGTATATTTTTCCC-3′
MJ0145 D183N	VBD334	5′-CATAGGTGGA*AAT*AACTTCATGGCTCCATCAAACGG-3′
	VBD335	5′-CCGTTTGATGGAGCCATGAAGTT*ATT*TCCACCTATG-3′
MJ0145 D138N	VBD336	5′-GGCTATGTTCAAATCGCTCATATT*AAT* ATAAACAACATTACTGGG-3′
	VBD337	5′-CCCAGTAATGTTGTTTAT*ATT*AAT ATGAGCGATTTGAACATAGCC-3′

[a] Underline denotes *Nde*I, *Ase*I, *Bfr*BI, and *Hin*dIII sites that were included in the primers to facilitate cloning. The bases in italic represent the inserted mutation, start, and stop codons.

nosine 5′-triphosphate (sodium salt hydrate) (GTP) was from Sigma. GTP stock solutions were prepared in 0.1 M potassium phosphate buffer (pH 6.8). $MgCl_2$ was obtained from Sigma. PCR reactions were carried out on an Eppendorf MasterCycler Gradient. Purifications were carried out on a GE Healthcare AKTA Fast Performance liquid chromatography apparatus. UV−visible spectra were acquired on an Agilent 8453 diode array spectrophotometer fitted with an eight-position cell changer. HPLC analysis used an Agilent 1100 series HPLC equipped with a photodiode array detector.

Cloning of GCH III from M. jannaschii. GCH III (MJ0145) was amplified from genomic DNA of *M. jannaschii*. Primers used in the PCR reactions are shown in Table 1 with the start, stop, and restriction sites indicated. Briefly, MJ0145 was amplified via PCR with Pfu turbo DNA polymerase. After the addition of a poly-A tail via Taq polymerase, each open reading frame (orf) was ligated into pGEM Easy-T vector for blue/white screening. Plasmids from various white colonies growing on plates containing 100 μg/mL ampicillin were isolated using a QIAGEN miniprep kit and sequenced via T7 and SP6 promoters by the University of Michigan DNA Sequencing Core. Once the sequence was verified, each orf was digested from pGEM Easy-T vector and ligated into pET28a and pET29a vectors.

Quickchange Mutagenesis of MJ0145 D183N and D138N. The D183N and D138N variants of MJ0145 were made from the primers reported in Table 1. The mutation and inserted restriction site are noted. Briefly, PCR reactions were carried out with the mutagenesis primers and a pET29a vector carrying MJ0145 according to the manufacturer's (Stratagene) protocol with annealing temperatures of 53−57 °C. After plasmid amplification of the mutant in XL1-Blue cells, sequencing was carried out (University of Michigan DNA Sequencing Core) to confirm the desired mutation.

Overexpression of Wild-Type MJ0145 and Site-Directed Variants in Escherichia coli. The pET29a vectors with the desired gene were transformed into electrocompetent BL21-(DE3) cells. A single colony from a plate containing LB medium and 34 μg/mL kanamycin was placed into 0.1 L of LB broth containing 34 μg/mL kanamycin and grown overnight. Six 2.8 L Fernbach flasks containing 1 L of LB medium and 34 μg/mL kanamycin were inoculated with an aliquot (~15 mL) of the overnight growth. Cells were grown at 37 °C to an $OD_{600\ nm} \sim 1$ prior to induction with addition of IPTG to 0.1 mM final concentration. Cells were pelleted 5 h after induction for wild-type and 8 h after induction for site-directed variants by centrifugation at 4000*g*, flash frozen in liquid N_2, and stored at −80 °C.

Overexpression of Selenomethionine-Labeled MJ0145 in E. coli. Cells from an overnight growth in 0.1 L of LB broth containing 34 μg/mL kanamycin were collected at 14 000*g* at 4 °C and resuspended in 0.1 L of M9 minimal media. Five 2.8 L Fernbach flasks containing 1 L of M9 minimal medium and 34 μg/mL kanamycin were inoculated with an aliquot (~20 mL) of the resuspension and grown essentially as described by Doublié (*14*) for expression under methionine pathway inhibition conditions. Cells were collected by centrifugation at 7000*g* at 4 °C from a growth at 37 °C after 8 h, flash frozen in liquid N_2, and stored at −80 °C.

Purification of GCH III, SeMet GCH III, and GCH III Variants. All purification steps were carried out at 4 °C. All steps were carried out in buffer A, which consisted of 0.02 M Tris·HCl (pH 8.0), 0.5 mM DTT, and additional components as indicated below. Cells (~20 g) containing overexpressed MJ0145 were suspended in 0.05 L of buffer A containing ~12 mg PMSF. Cells were disrupted using a Branson sonifier with 20 s bursts at 60% power with 1 min rest periods for a total of 5 min. The temperature of the extract was kept at <10 °C throughout the sonication process by keeping the cells on ice. Cleared lysates were obtained by centrifugation at 15000*g* for 45 min. The extract was loaded onto a Q-Sepharose fast flow column (2.5 × 15 cm) that had been equilibrated with buffer A and washed with 0.16 L of the same, and the protein was eluted with a 0−0.5 M gradient of KCl in buffer A. Fractions containing the desired protein (as determined by SDS−PAGE) were pooled and mixed, over a period of 20 min, with an equivalent volume of buffer A containing 2 M $(NH_4)_2SO_4$. The resulting solution was loaded onto a Butyl Sepharose 4 Fast Flow column (2.5 × 15 cm) that had been equilibrated with buffer A containing 1 M $(NH_4)_2SO_4$. The protein was eluted with a gradient (0.5 L) from 1 to 0 M $(NH_4)_2SO_4$ in buffer A. Fractions containing the desired protein were pooled and dialyzed (12−14 kDa molecular mass cutoff) against 2 L of buffer A with one change. MJ0145 was concentrated using an Amicon pressure concentration device (YM-10 membrane). Aliquots of the resulting protein were frozen in liquid N_2 and stored at − 80 °C. Each of the proteins studied here were purified in a manner similar to that described above for the MJ0145 protein with one exception. SeMet MJ0145 was purified in the presence of 10 mM DTT to minimize oxidation of the SeMet residues (*14*). Aliquots of the native

protein used in some of the crystallization experiments were treated with a Chelex resin (Na^+ form, 1 × 20 cm) equilibrated buffer A.

Protein stocks were quantified with a BCA protein assay kit (Pierce) using bovine serum albumin as the standard. Because of the DTT content (10 mM), the SeMet-containing MJ0145 was quantified using a Bradford protein assay kit (Bio-Rad) with bovine serum albumin as a standard.

Metal Ion Determination. The metal content of each of the proteins was determined by ICP-OES at Garratt-Callahan Co. (Burlingame, CA).

Monitoring Turnover of MJ0145 with GTP. The assay solutions contained 0.5 μM protein in a solution containing 0.2−1 mM GTP, 0.1 M Tris·HCl (pH 8.0), 0.5 M NH_4Cl, 5 mM DTT, and 10 mM $MgCl_2$, in a total volume of 0.5 mL. The solutions were equilibrated at 70 °C prior to the addition of GTP to initiate the reaction. Samples (0.1 mL) were withdrawn at various times (1−5 min) after addition of GTP and quenched by cooling on ice. The assay mixtures were filtered through Microcon (Millipore) centrifugation filtration devices (YM10) at 7000*g* for 8 min at room temperature. An aliquot (0.1 mL) was analyzed by HPLC using a Zorbax SAX column (4.6 × 150 mm) from Agilent Technologies as described previously (*15*). For the analysis, the column was equilibrated with a solution containing 1% (v/v) of 0.75 M $NH_4H_2PO_4$ dissolved in water containing 2% (v/v) acetonitrile, at a flow rate of 0.75 mL/min. Products were eluted with two successive gradients of the initial buffer 1−15% (over 20 min) and 15−95% (over 5 min) in water. Previously determined standard curves of FAPy were used to quantify the product.

Crystallization and Structure Solution. Crystals of both native and selenomethionine-substituted protein were grown using the hanging drop method. The selenomethionine-substituted crystal was grown by mixing 2 μL of a solution containing 10 mg/mL protein and 2 mM GTP (dissolved in 0.1 M potassium phosphate buffer, pH 6.8) with 2 μL of a solution containing 80 mM potassium phosphate, 19% PEG 8000 (pH 6.5) and equilibrated against the PEG solution. Crystals of the native protein/GTP complex were grown in the same fashion, except that the precipitant solution contained 16% PEG 4000, 0.2 M sodium acetate, and 0.1 M Tris·HCl (pH 8.5). Crystals grow in 3−4 days under both conditions.

A crystal of the selenomethionine-substituted protein was immersed in a solution of 35% PEG 8000 and flash frozen in liquid N_2. Diffraction data at three wavelengths for MAD phasing were collected at SSRL, beam line 9-2, using a MAR 325 detector. The crystal diffracted to 2.8 Å, but had mosaicity estimated at >2°. Data were reduced using CrystalClear (*16*). Using space group *I*222, SOLVE (*17*) found 12 of 16 possible Se atoms. Density modification with RESOLVE (*18*) produced an electron density map into which the polypeptide chain was built by Buccaneer (*19*). Side chains could be seen and identified for ∼40% of the amino acid residues. A large ligand, presumably GTP, was clearly present, but its identity could not be determined.

A crystal of the native protein was mounted in a capillary, and data were collected at room temperature using a Rigaku RAXIS IV^{++} image plate detector mounted on a Rigaku RU-H3R generator with Confocal-Blue optics. Data were reduced and scaled using CrystalClear (*16*). Molecular replacement was performed using PHASER (*20*) with the partially built model from the selenomethionine protein (476 residues in two protein chains, 40% with side chains and 60% represented as alanine) as the search model. PHASER placed two copies of the search model in the unit cell and the remainder of the model, including missing side chains, was built into a map calculated using phases from PHASER by ARP/WARP (*21*). The model was completed by hand; GTP and metal ions were added using Coot (*22*) and refined with REFMAC5 (*23*). Residues 252−268 are disordered and not modeled. Refinement statistics are summarized in Table 2. Figures were prepared using PYMOL (*24*). Other calculations, including the buried surface area, were carried out with the CCP4 package (*25*).

Table 2: Crystallographic Data Collection and Refinement

	selenomethionine protein	native
crystal class, space group	orthorhombic, *I*222	*P*21212
cell parameters (Å)	*a* = 91.1	*a* = 100.2
	b = 100.3	*b* = 129.6
	c = 126.2	*c* = 90.9
Z (molecules/au)	2	4
temperature (K)	100	292

	selenomethionine protein			
	peak	remote	inflection	native
wavelength (Å)	0.9791	0.9116	0.9793	1.54
resolution (Å)	2.75	2.8	2.8	2.0
total refls	203 437	203 701	203 763	272 154
unique refls	30 624	30 116	29 817	76 172
multiplicity[a]	6.6/5.7	6.7/5.7	6.7/5.5	3.5/3.6
completeness (%)[a]	98/98	98/98	98/98	95/93
mean $I/\sigma(I)$[a]	9.2/2.5	11.0/3.0	9.8/2.7	9.0/2.9
R_{merge}[a]	0.12/0.43	0.11/0.46	0.11/0.50	0.08/0.42
FOM (SOLVE)		0.51−2.8 Å		
R_{cryst}/R_{free}				0.21/0.25
rmsd bonds (Å)/ angles (deg)				0.014/1.52
no. of residues protein/water				1008/193
Ramachandran plot[b] (%)				96.7/3.3
avg B (Å^2) protein				27.0
avg B (Å^2) GTP/ metal ions				24.0
avg B (Å^2) water				32.0

[a] Overall/outermost shell. [b] Residues in most favorable/other allowed regions.

RESULTS

Cloning, Purification, and Turnover of MJ0145. The GCH III protein of the methanogenic archaeon *M. jannaschii* (MJ0145) was cloned, overexpressed in *E. coli*, and purified to homogeneity by anion exchange and hydrophobic interactions chromatography. Previous studies have shown this protein to be most active at elevated temperatures (∼70 °C); activity assays at 70 °C confirm the reported GTP→FAPy activity of MJ0145. Furthermore, the k_{cat} for the protein is similar to the value reported in the literature (Table 3) (*5*). The protein was subjected to metal analysis to determine if a tightly bound zinc metal ion was present. In contrast to both GCH I and GCH II (*9*, *10*, *12*), GCH III is devoid of zinc under conditions where we routinely detect equimolar quantities of Zn^{2+} in preparations of GCH II in the laboratory

Table 3: Turnover Number and Zinc Content of Wild-Type and Asp183Asn and Asp138Asn Variants of GCH III

protein	turnover number (min^{-1})	Zn (mol/monomer)
GCH III	13.2 ± 2.5	<0.125
Asp183Asn GCH III	$1.3 \pm 0.2 \times 10^{-3}$	<0.125
Asp138Asn GCH III	$1.2 \pm 0.3 \times 10^{-3}$	<0.125

(Table 3) (*7*). However, calcium was detected up to ~10-fold in molar excess of the protein; treatment of the protein with Chelex (Na^+ form) reduced the Ca^{2+} to 4-fold excess but did not eliminate it; the Chelex-treated native protein was used in the structure reported here. Gel filtration studies with the protein preparation used in these studies are also most consistent with a tetramer composition and not a trimer, as has been reported (*5*). The X-ray crystal structure of the protein described in this paper confirms GCH III is a tetramer.

Crystallization and Structure Solution. We obtained large square orthorhombic crystals containing the GCH III/GTP complex when both GTP and potassium ion are present in the crystallization drop and when magnesium, which has been shown to be required for activity (*5*), is absent. Although we have been unable to obtain high-resolution data from frozen crystals, we were able to solve the structure using three-wavelength MAD phasing from a poorly diffracting crystal containing selenomethionine-substituted GCH III and to complete model building and refinement using a 2.0 Å resolution data set collected at room temperature. There are four independent molecules in the crystallographic asymmetric unit, and we find GTP and three metal ions bound at full occupancy in all four independent molecules.

Protein Structure, Fold, and Oligomerization State. GCH III is a tetramer of identical subunits. As shown in Figure 2A, each protein chain folds into two domains. The clam-shell-like structure of each chain is obtained by head-to-tail fusion of two successive N-$\beta\alpha\alpha\beta\beta\alpha\beta\alpha\beta$-C domains. Within each domain, $\alpha_1\alpha_4$ and $\alpha_2\alpha_3$ bookend a central antiparallel β-sheet formed by strands 1−5, forming a ferredoxin-like $\alpha-\beta-\alpha$ sandwich. Despite limited sequence similarity (Figure 2C, ~18% identity), the three-dimensional structures of the N- and C-terminal halves of each monomer (amino acids 1−131 and 132−251, respectively) are readily superimposed (Figure 2B) to reveal identical folds (rmsd 1.3 Å). The high degree of structural identity between the N- and C-terminal halves suggests that GCH III arose through a gene duplication−fusion event. The possible similarities between portions of the N- and C-terminal halves of GCH III had been suggested on the basis of primary and secondary structure predictions (*5*).

Two monomers form a tightly interdigitated dimer (Figure 2D) with the substrate binding site located at the interface between two subunits. Two dimers further associate to form a tetramer, as shown in Figure 2E. The tetramer is organized such that the N-terminal domains are on the inside and the C-terminal domains, containing phosphate binding residues, are on the surface of the tetramer. There are no significant structural differences between the protein chains; the rms deviation of α-carbon atoms between any two protein chains is 0.2 Å. The dimer−dimer interface of GCH III is extensive: ~2000 $Å^2$ surface area from each dimer is buried.

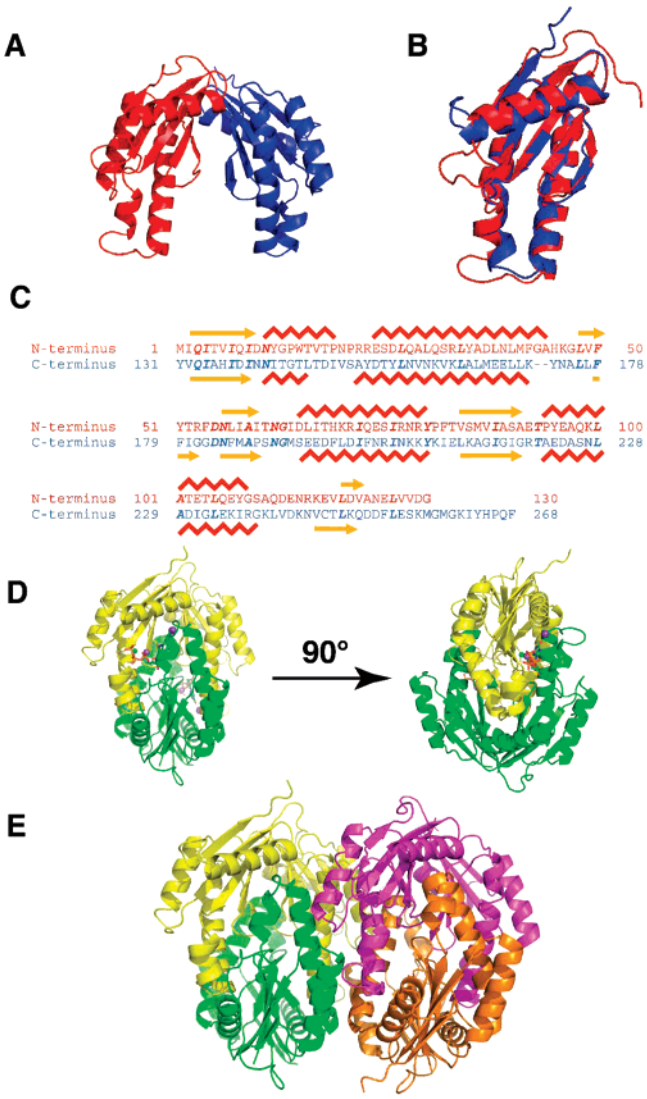

FIGURE 2: Structure of GCH III. (A) A single protein chain showing the N-terminal (red) and C-terminal (blue) domains. (B) Superpositions of the N- (red) and C-terminal (blue) halves of the protein showing the structural identity. (C) The N- (red) and C-terminal (blue) halves of GCH III lack discernible sequence identity (bold italic). The two Asp residues (138 and 183) that coordinate the metal ions at sites 1 and 2 are shown by arrows. (D) The tightly interdigitated dimer (chains A and C) are shown in two views; GTP and the metal ions are shown as sticks and spheres, respectively. (E) GCH III is a tetramer in the crystal. The dimer−dimer interface is composed of residues from the N-terminal domains of all four chains.

The quaternary structure does not result from the presence of GTP; a low-resolution structure of the protein without substrate in a different crystal form contains the same tetramer structure (S. Roberts, V. Bandarian, unpublished observations). The tetramer observed in the structure is consistent with the gel filtration studies reported above.

A DALI search (*26*), utilizing either the complete monomer or the N- or C-terminal half of the protein, revealed similarity between the repeating sandwich halves of GCH III and a so-called palm domain, which houses the catalytic site of several DNA polymerases. A palm domain is also present in adenylyl cyclase (*27*−*31*) and diguanylyl cyclase (*32*). The homology of the palm domains of these proteins has been noted in the literature (*33*−*36*). In the following discussion, we will highlight the similarities between GCH

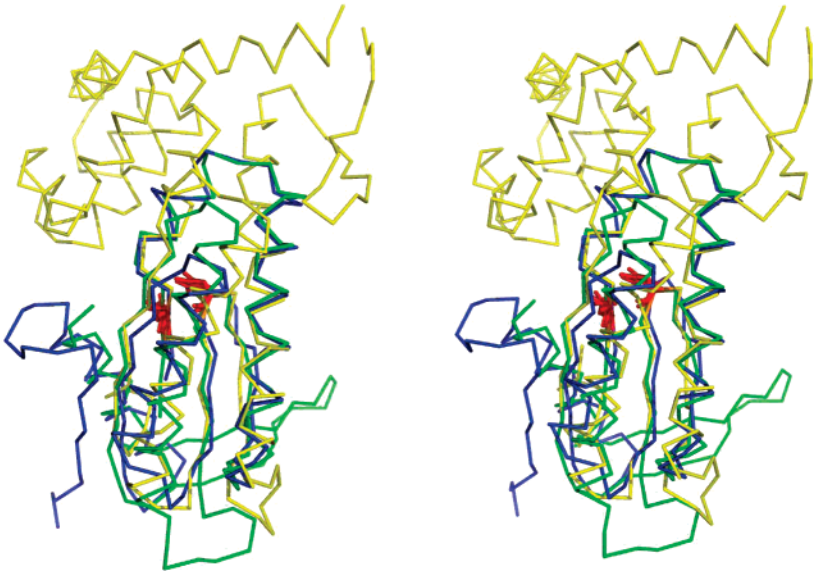

FIGURE 3: Superposition of GCH III (green) with similar domains from T7 polymerase (1T7P, yellow) and adenylyl cyclase (1CJK, blue), shown in stereo. The Asp residues that bind the phosphate oxygen atoms of the substrate are shown in red.

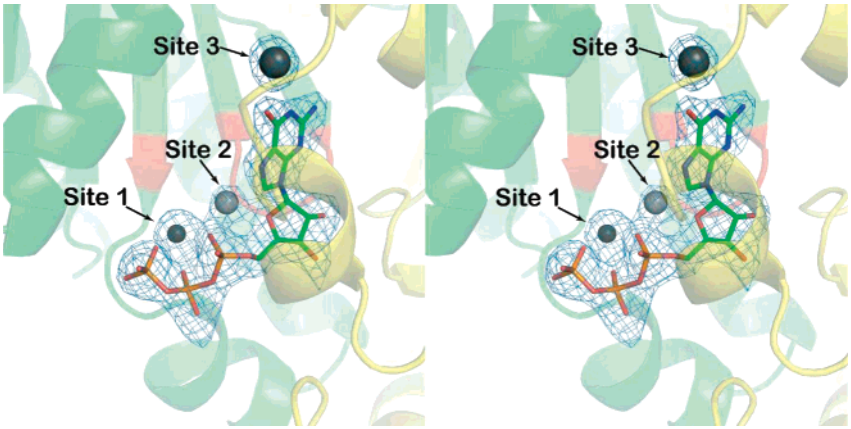

FIGURE 4: Stereodiagram showing electron density ($F_o - F_c$ omit map contoured at 3σ) around GTP and the three metal ions in the active site of GCH III. The omit map was calculated after refinement with Refmac (*23*) of a model omitting all copies of GTP and metal ions. Each active site is composed of residues from two subunits (green and yellow). The positions of the GGDN loop and invariant Asp residues are colored in red.

III and these proteins using a subset, represented by T7 DNA polymerase (*37*) and adenylyl cyclase (*29*, *30*), for clarity.

A structural superposition of the C-terminal half of GCH III, which contains the eponymous GGDN sequence, and representative palm domains from the PDB is shown in Figure 3. Intriguingly, the structural alignments also reveal possible mechanistic analogies between GCH III and other palm domain containing proteins. All of the palm domains shown in Figure 3 bind nucleotides and/or DNA as substrate and have been proposed to catalyze phosphodiester bond cleavage in a mechanism that utilizes two divalent metal ions (*38*−*40*). Two widely conserved Asp residues have been found in the active sites of all palm-containing proteins that catalyze phosphodiester hydrolysis in the course of turnover. The carboxylate side chains of these residues are ligands to two metal ions, which are essential for catalysis (*30*). The catalytically active divalent metal ions in these proteins are generally Mg^{2+}; however, other metals ions, such as Zn^{2+}, Ca^{2+}, or Na^{+}, have been reported to occupy these sites (*30*, *37*, *41*, *42*). Interestingly, these aspartate residues (Asp 183 and 138) are conserved in GCH III as well and found in essentially the same location in its structure, suggesting a functional link between the mechanisms of action of these widely different enzymes (see red residues in Figure 3).

GTP Binding, Metal Ions, and Active Site Architecture. Crystals of GCH III were grown in the presence of GTP and clear difference electron density for GTP and three metal ions was observed in all four subunits. (Figure 4). The thermal parameters of the ligands and metal ions are equal to or lower than those of the surrounding protein residues, an indication of full occupancy of the binding sites. The substrate binding site lies between two protein chains of the interdigitated dimer (either A and C or B and D). The guanosine base is located near the conserved GGDN sequence motif with the base surrounded by protein residues while the end of the triphosphate is solvent-exposed. In addition to GTP, the difference electron density revealed the presence of three metal ions (Figure 4), which will hereafter be denoted sites 1−3. As discussed below, calcium, sodium, and potassium have been modeled into sites 1−3, respectively.

Each of the metal ions has extensive interactions with active site residues and the substrate GTP (Figure 5A,B). The metal ions in sites 1 and 2 are bound to triphosphate

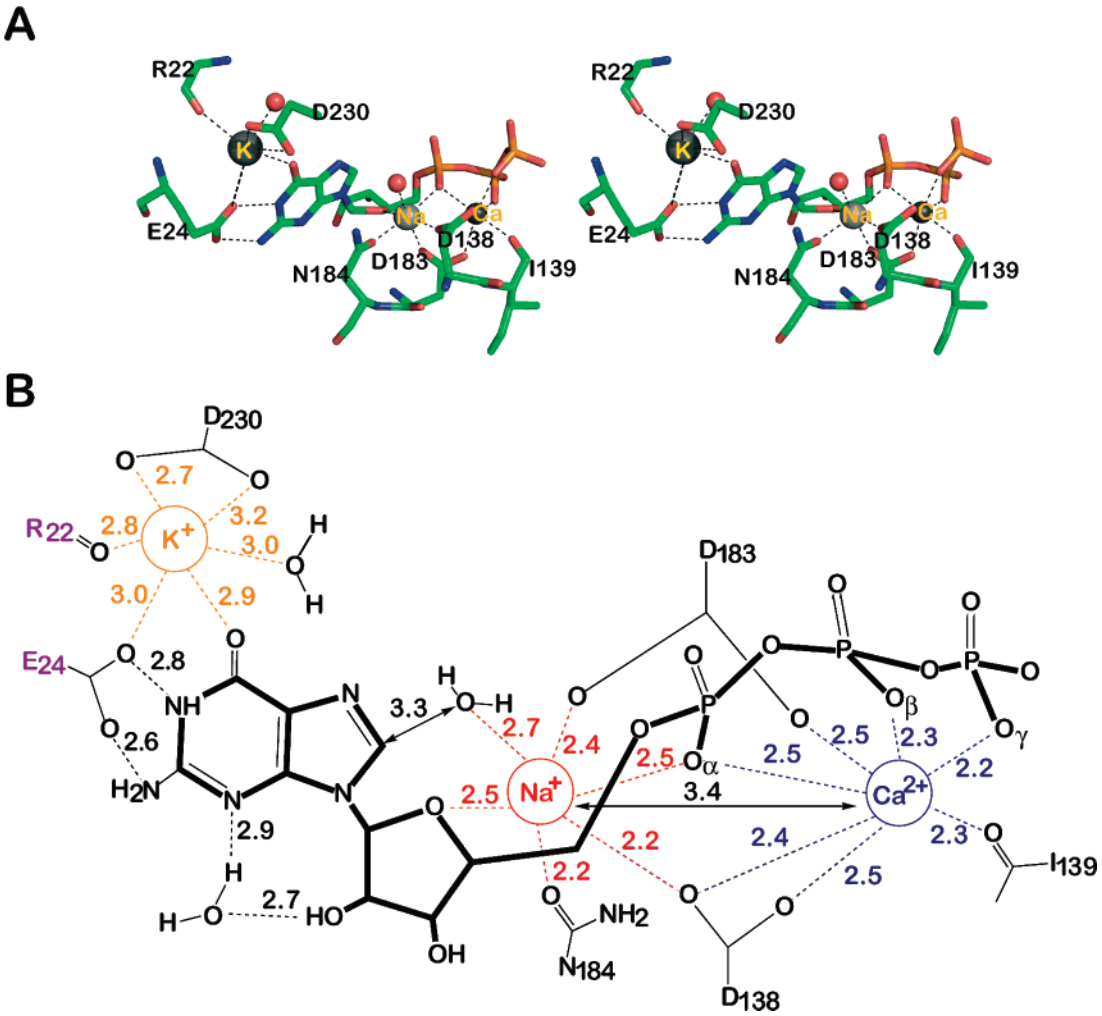

FIGURE 5: GTP and metal ion binding to GCH III. (A) Stereoview of GTP in the active site showing the metal ion−substrate and metal ion−protein interactions. (B) A schematic of interactions among active site residues, the metal ions, and the substrate. The Ca^{2+}, Na^{+}, and K^{+} have been referred to as Sites 1, 2 and 3 in the text, respectively.

oxygen atoms in a manner that is similar to that observed with enzymes that utilize two metal ions to carry out phosphodiester cleavage (see above). The third metal ion is unique to GCH III; it is bound to O6 of GTP and several protein residues (Figure 5).

In addition to interactions with the metal ions, GTP makes a large number of specific interactions with residues contributed by both protein chains. The key binding interactions are summarized in Figure 5B. Notably, nearly all conserved residues in annotated GCH III proteins are found to be in the active site and interact with either the GTP or the bound metal ions.

A conserved GGDN motif in a group of archaea proteins has been used as the basis for classifying MJ0145 into COG2429 and Pfam05165. This conserved GGDN motif, residues 181−184 in MJ0145, lies on a loop between two β-strands in the active site of the protein and provides ligands to the site 1 and site 2 metal ions. Asp183 is itself bound to both the site 1 and site 2 metal ions, while the adjacent Asn184 is involved in a complex network of interactions; in addition to being bound to the site 1 metal ion through its side chain oxygen OD1 (distance 2.2 Å), the side chain ND2 is hydrogen bonded to the side chain of His136, which in turn is hydrogen bonded to Asp230, the carboxylate side chain of which is bound to the site 3 metal ion. In addition to these residues, Glu24 of the adjacent dimer subunit, which also lines the active site cavity, is located near the site 3 metal ion. Glu24 forms hydrogen bonds with N1 and N2 of the GTP and is probably important for substrate recognition and specificity. The second Asp residue (Asp138), whose position appears to be conserved in GCH III and other palm domain containing proteins, is nearby and bridges the site 1 and 2 metal ions.

Metal Ion Identities and Coordination Geometries in the Active Site of GCH III. The identities of metal ions observed in GCH III have been tentatively assigned after considering biochemical information, available metal ions, apparent electron density, and observed coordination geometries. GCH III requires both a divalent, and a monovalent cation for activity (*5*); the crystallization drops contained 0.2 M sodium acetate as the precipitant, Ca^{2+} from the protein preparation (metal analysis shown above), and K^{+} arising from the GTP stock solution.

At 2 Å resolution, if metal sites are fully occupied, one can distinguish a heavier metal, such as Ca^{2+} or K^{+} from Na^{+} or Mg^{2+}, both of which have electron densities similar to that of water; however, Ca^{2+} cannot be distinguished from K^{+} by electron density alone. Unrestrained metal−oxygen bond distances are not reliably determined at 2 Å resolution, but the mean metal−oxygen bond distance, which is

determined by the size of the cavity the metal is occupying, is more reliable. Searches of the Cambridge Data Base (*43*) show mean metal−oxygen distances for available metal ions to be Ca^{2+} = 2.4 Å, Na^{+} = 2.4 Å, and K^{+} = 2.8 Å. Thus, substitution of potassium for calcium will increase the size of the metal coordination sphere by ~0.8 Å, a difference apparent at 2.0 Å resolution.

The site 1 metal is probably Ca^{2+}. Although Ca^{2+} was not explicitly added to the crystallization conditions, metal analysis (described above) has shown that the protein stock used for crystallization contains significant amounts of Ca^{2+}. It has been shown that Ca^{2+} inhibits activity, consistent with presence of unreacted substrate in the active site (*5*). The calcium in site 1 is coordinated by one oxygen atom from each of the α-, *β*-, and *γ*- phosphates of GTP, while the remaining sites are occupied by carboxylate oxygens from each of the conserved Asp183 and Asp138, and a main chain carbonyl oxygen of Ile139.

The site 2 electron density is consistent with full occupancy by Na^{+}. The site 2 metal ion has five ligands. Two are contributed from atoms of GTP including the α-phosphate and the ribose oxygen, and the remaining three by carboxylate oxygen atoms from Asp 138 and Asp 183 and the amide nitrogen of Asn 184. Electron density for a water ligand in the sixth coordination position of site 2 is seen in three out of four monomers.

The metal at site 3 is clearly a potassium ion. This site could also accommodate an ammonium ion, the other monovalent ion reported to stimulate activity (*5*). As noted above, K^{+} is required to obtain crystals of the protein/GTP complex. The potassium ion is surrounded by oxygen atoms from the side chain of Asp230 from one subunit, the main chain oxygen of Arg22, the carboxylate side chain of Glu24 from the adjacent subunit in the dimer, O6 of GTP, and a water molecule. The potassium site appears to be used for substrate recognition, but it may also be involved in a catalytic capacity (see Discussion). This site is >7 Å away from sites 1 and 2, whose role we suspect to be largely catalytic by analogy to the two metal ion mechanisms that have been proposed for analogous sites in other enzymes (see Discussion).

An anomalous Fourier map calculated using the native data set (X-ray wavelength = Cu Kα = 1.54 Å) is consistent with these metal assignments. Although the map is noisy, peaks (3.5−7σ) are present at the eight sites identified as Ca^{2+} or K^{+} ions and absent at the four sites assigned as Na^{+} ions.

Site-Directed Mutagenesis of D138 and D183 in GCH III. The structure reveals several amino acids in proximity of the substrate that could be involved in catalysis. Two in particular, Asp138 and Asp183, are highly integrated into the metal coordination at sites 1 and 2. Site-directed mutations of the analogous Asp residues in structurally homologous palm domains lead to substantial diminution of catalytic activity (*30*, *38*). To determine the extent to which Asp138 and Asp183 contribute to catalysis, each of the residues were mutated to Asn, and the variants were purified and assayed for ability to convert GTP to FAPy. Consistent with their position in the active site of the protein, the Asp→Asn variants of these residues are impaired ≥10^4 in the conversion of GTP to FAPy, as assayed by HPLC analysis of reaction products (see Table 3), suggesting that these residues are absolutely required for activity. Therefore, the phenotype of the Asp variants of GCH III is identical to the effect of the analogous mutations in palm domains in other proteins.

The structural results also allow interpretation of a previous site-directed mutagenesis study. White and co-workers (*5*) have shown that His136, which is conserved, is important for catalysis; the k_{cat} of the His136Gln variant of GCH III is reduced 15-fold relative to the wild-type protein, but the K_M for GTP is comparable to the wild-type. His136 is involved in a network of interactions that involve Asn184 and Asp230, which bind site 2 and 3 metal ions, respectively. One may imagine that this variant disrupts the complex network and therefore affects binding of potassium to site 3; however, the effect of the mutation on the affinities of the protein for the metal ions is not known.

DISCUSSION

Mechanism of GCH III. The X-ray crystal structure of GCH III from *M. jannaschii* has produced several unanticipated revelations, perhaps the most unexpected being an active site geometry that appears to be well-suited for two metal ion catalysis. Two metal ion catalysis was postulated to account for the reactions that are catalyzed by a large number of structurally different enzymes that employ two divalent metal ions for phosphoryl transfer reactions (*38*). We note in passing that two metal ion assisted catalysis of this type has also been proposed for reactions catalyzed by structurally distinct restriction endonucleases (*42*, *44*) and alkaline phosphatase (*45*), as well as RNA-based phosphotransferases (*38*, *46*). However, since GCH III catalyzes both a cyclohydrolase as well as a phosphotransferase reaction, this structure extends the repertoire of enzymatic transformations that are associated with this metal ion arrangement and the particular fold associated with GCH III.

A putative mechanism for GCH III that is consistent with the biochemical and structural findings to date is shown in Figure 6. Although the Ca^{2+}/Na^{+}-occupied structure solved here is almost certainly an inhibited form of the protein, by analogy to two metal ion catalysis mechanisms that have been proposed (*38*), we posit that the metal ion(s) (magnesium ions in the active protein) act as Lewis acids to activate a water molecule to initiate the cyclohydrolase chemistry. Attack of the water molecule at C-8 leads to formation of a tetrahedral adduct. Such a step requires protonation at N-7 of the substrate. Although a general acid catalyst is not obvious near N-7, we note that in addition to the water molecule coordinated to site 2, which is 3.3 Å from N-7, an ordered water molecule is also located ~ 2.9 Å from N-7 of the substrate in chain A. Both water molecules hydrogen bond with the conserved Arg237, which may serve a dual role in catalysis by positioning and facilitating activation of the nucleophile required in the early phase of the reaction, as well as the second water molecule, which may be involved in protonation of N-7 as the chemistry proceeds. In addition, the side chain oxygen of Thr16 is ~3.2 Å from N-7; although the pK_a is not appropriate for protonation, hydrogen-bonding interactions between the side chain of Thr16 and N-7 may stabilize the developing negative charge and reduce the energy of the transition state. In the second half-reaction, collapse of the tetrahedral adduct concomitant with proto-

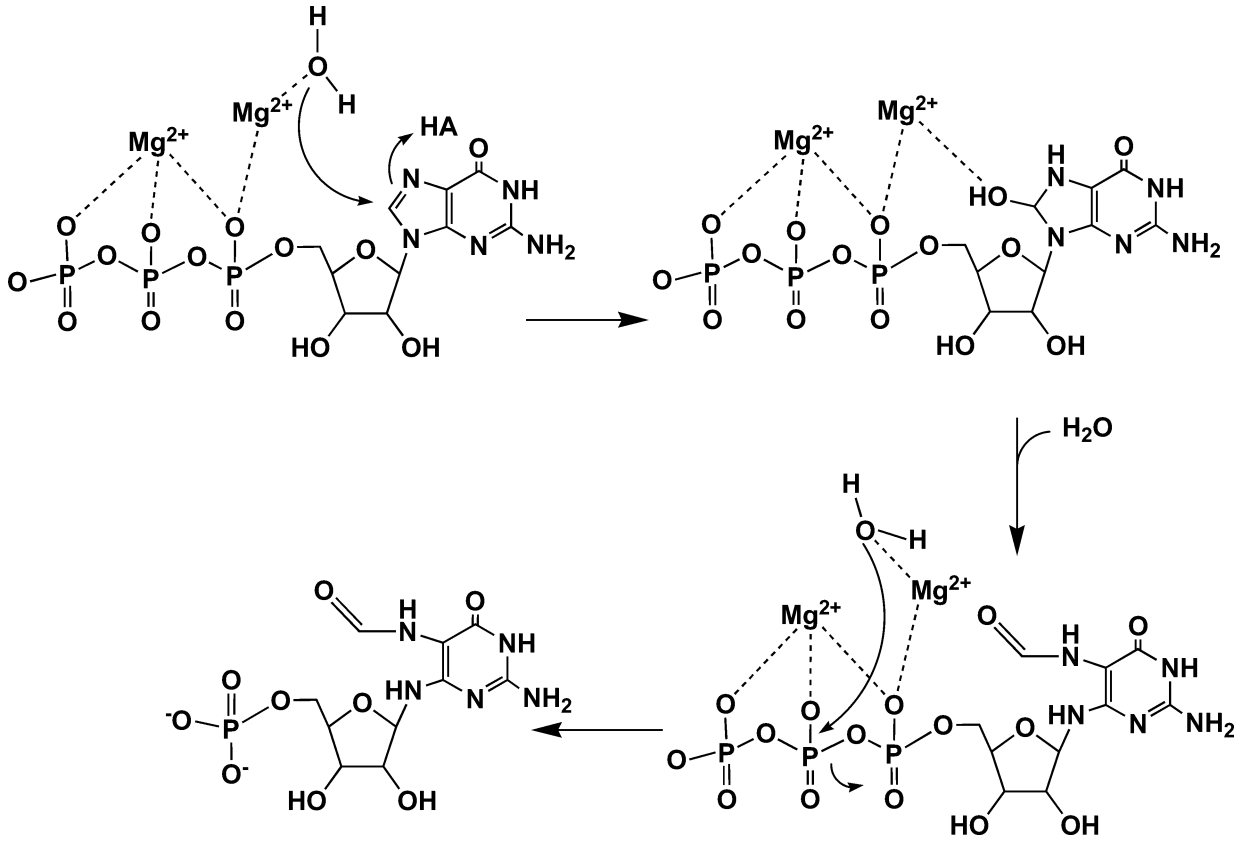

FIGURE 6: Proposed mechanism for GCH III. The divalent cations activate a water molecule for attack at C-8 of the substrate forming a tetrahedral adduct, which collapses to the formamide product. In this figure, cyclohydrolase chemistry is shown to *precede* phosphodiesterase; however, this need not be the case.

nation at N-9 leads to formation of the FAPy product. This step, however, need not be catalyzed and can take place in solution. The structure does not reveal obvious residues or ordered water molecules in the vicinity of N-9 that could act as general acid catalysts in this half-reaction. In Figure 6, the cyclohydrolase chemistry is shown to precede the dephosphorylation, which must occur since a monophosphorylated product is produced by GCH III; at this point, the order of these steps is not known and the reverse is also plausible.

Dephosphorylation of GTP in the course of its conversion to APy or FAPy occurs in the reactions catalyzed by the structurally unrelated GCH II as well. Formation of a GMP• GCH II covalent adduct, which precedes the cyclohydrolase chemistry, has been proposed (*47*). However, formation of the covalent adduct has not been demonstrated experimentally. On the basis of the X-ray structure of GCH II, Arg128 was proposed to be the nucleophile (*12*); however, the role of this residue has not been confirmed. We do not observe a nucleophile near the β-phosphate of GTP that could be involved in covalent catalysis in GCH III. However, one cannot rule out that in the catalytically competent binary complex a conformational change may place a residue in the appropriate location. Studies on the stereochemistry of the cleavage reaction with GCH II and GCH III may be useful in determining the course of the reaction. We note that GCH I catalyzes the Mg^{2+}-independent cleavage of C-8 and does not catalyze hydrolysis of the triphosphate moiety of GTP, suggesting that the hydrolysis is not an obligatory step on the pathway to hydrolysis of C-8 in nature.

In addition to the apparent structural role, a catalytic role of the potassium at site 3 remains to be established. One may envision, for instance, that the potassium ion polarizes O6 of GTP, leading to increased electrophilicity at C-8 of the substrate. Alternatively, site 3 could be responsible for organizing a network of water molecules to protonate N-7, where negative charge will develop as C-8 undergoes nucleophilic attack.

Comparison of GCH III to GCH I and GCH II. We initiated structural studies on GCH III because we were intrigued by the observation that conversion of GTP to FAPy is catalyzed by a GCH II ortholog in *S. coelicolor* (SCO 6655), which has substantial sequence identity (40% to *E. coli* GCH II) to enzymes that catalyze canonical GCH II chemistry (GTP→APy) and no sequence similarity to GCH III. Furthermore, it had been shown in the literature than while GCH III is a Mg^{2+}-requiring enzyme (*5*), GCH II is a zinc-containing protein (*9*, *10*). Biochemical studies from our lab had demonstrated that the fate of GTP (FAPy or APy) in the reaction catalyzed by noncanonical GCH II from *S. coelicolor* is dictated by a single amino acid. A Tyr residue (Tyr105) that is 4.3 Å from N-7 of the substrate and forms a hydrogen bond to the water molecule, which is a ligand to the active site Zn^{2+}, dictates the fate of GTP. This Met residue is a Tyr in all proteins (including the two additional intragenomic homologs of GCH II in *S. coelicolor*) that carry out the canonical GTP→APy reaction; the Met120Tyr variant of SCO 6655 catalyzes the canonical reaction (*7*). However, in the absence of structural information on GCH III, it has been difficult to determine a link between SCO 6655 and

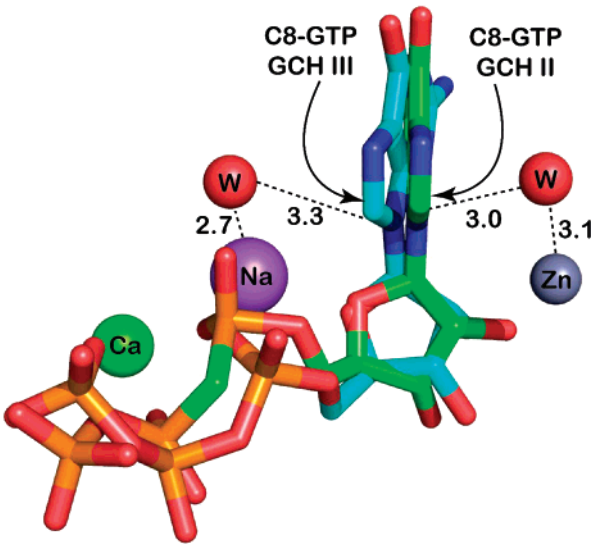

FIGURE 7: Comparison of GTP bound to the active site of GCH II and GCH III. In each case, the metal ion in the active site binds a water molecule that is near the C-8 of the substrate.

GCH III, in an attempt to determine if convergent evolution of activity has taken place.

The structure of GCH III clearly demonstrates that SCO 6655 and GCH III have evolved the same activity by convergent evolution. These proteins have distinctly different structures. In addition, the "switch" residue that we had identified in SCO 6655 is absent in GCH III. Additional evidence for convergent evolution of function is obtained by comparing the manner in which substrate is bound to the active site and presented to the "catalytic" water molecule. As shown in Figure 7, while the water molecule is nearly equidistant from the C-8 of GTP in each (3.0 and 3.3 Å in GCH II and GCH III, respectively), it is on the *opposite* face of the base. The superposition predicts that the initial tetrahedral adduct in GCH III would have *R*-stereochemistry at C-8, whereas in GCH II the initial adduct would be the *S*-isomer. Stereochemical information, however, is lost upon the formation of the formamide product.

Discovery of a Cyclohydrolase Activity in a Palm Domain. The X-ray structure of GCH III reveals that it is a new member of a class of proteins with diverse biological roles ranging from DNA synthesis to production of cyclic nucleotides. The α−*β*−α sandwich region that GCH III has in common with all of these proteins was first observed in the structure of the Klenow fragment of DNA polymerase I (*48*), which resembles a right-hand with the DNA strand and nucleotide binding in the so-called palm region. Palm domains have been observed in DNA/RNA polymerase (*37*, *48*) and adenylyl cyclase (*29*, *30*, *39*, *40*) and have been proposed to a share common ancestor (*34*, *49*). To our knowledge, however, GCH III is the first protein with a palm-like fold that, in addition to phosphodiester hydrolysis, also catalyzes a cyclohydrolase reaction. Therefore, our discovery extends the chemical repertoire of proteins containing palm domains to include cyclohydrolase chemistry.

Many proteins containing palm domains catalyze the hydrolysis of a phosphodiester bond in the course of catalysis. Representative palm domains from GCH III, adenylyl cyclase, and T7 DNA polymerase bound to their respective substrate/substrate analog and divalent metal ions are shown in Figure 8. Despite substantial differences elsewhere in the structures, the palm domains of each are homologous. Each protein binds two divalent metal ions to two invariant aspartate side chains in the palm for catalysis. Although sodium and calcium were found to occupy these positions in the active site of GCH III in the current structure, we believe that, in the active form of the protein, two magnesium ions are used. In the active site of each protein, one metal ion (site 1 in GCH III, metal B in DNA polymerase and adenylyl cyclase) makes direct interactions with oxygen atoms from the phosphate moiety of the substrate, as well as the two invariant aspartates (Asp138 and Asp183 in GCH III) and a backbone carbonyl. There is remarkable consistency in the coordination sphere for this metal across the divergent protein structures. In general, one ion is bound to one oxygen atom from each of the three phosphate groups. A second metal ion (site 2 in GCH III, metal A in DNA polymerase and adenylyl cyclase) interacts with the two invariant aspartates and is involved in activating an incoming oxygen nucleophile, which is either the 3′-OH of a ribose or a water molecule.

By contrast to the remarkable conservation of the binding interactions that immobilize the triphosphate tail of the substrate in these structurally related proteins, the binding interactions between the purine ring of the substrate, but most importantly, the *position* of the purine ring relative to the ribose phosphate, are not conserved. Each of the proteins shown in the Figure 8 has acquired means of carrying out the chemistry on the bound substrate by modification in the position of the ribose and base moiety relative to the position of the two metal ions that bind and activate the substrate. For instance, in DNA polymerase, the incoming 3′-OH nucleophile of the growing polynucleotide chain is placed in the vicinity of the incoming nucleotide. Binding and stacking interactions are likely important in immobilizing the substrates in the correct position for chemistry. By analogy, 3′-OH of the ribose serves as the nucleophile in the adenylyl cyclase-catalyzed intramolecular cyclization reaction. In this case, the ribose and base are immobilized in a configuration appropriate for this chemistry. The activated nucleophile attacks the α-phosphate of the substrate to generate product. The binding site for the base/ribose duo places the nucleophile in a position required for chemistry. In GCH III, the base/ribose are rotated such that the C-8 of the substrate is in close proximity to the activated water molecule at site 2.

Does the Dephosphorylation Catalyzed by GCH III Result from Promiscuity? One may argue that formation of a monophosphorylated product may have been desirable to fulfill the substrate preference(s) of downstream biosynthetic enzymes. However, it may also represent a promiscuous side reaction. The evolution of new enzymatic activities has been proposed to require duplication of an existing enzyme followed by evolution and selection to achieve desirable traits. It has been postulated that enzyme evolution can take advantage of the promiscuous nature of enzymatic reactions by selecting for mutations that lead to improvements in efficiency (k_{cat}/K_M) of a side reaction that simultaneously reduces the efficiency of the parental reaction (*50*, *51*). An advantage of this approach is that the new and the old activities can coexist and that, as required, the old activity can be selected readily if evolutionary pressures require its

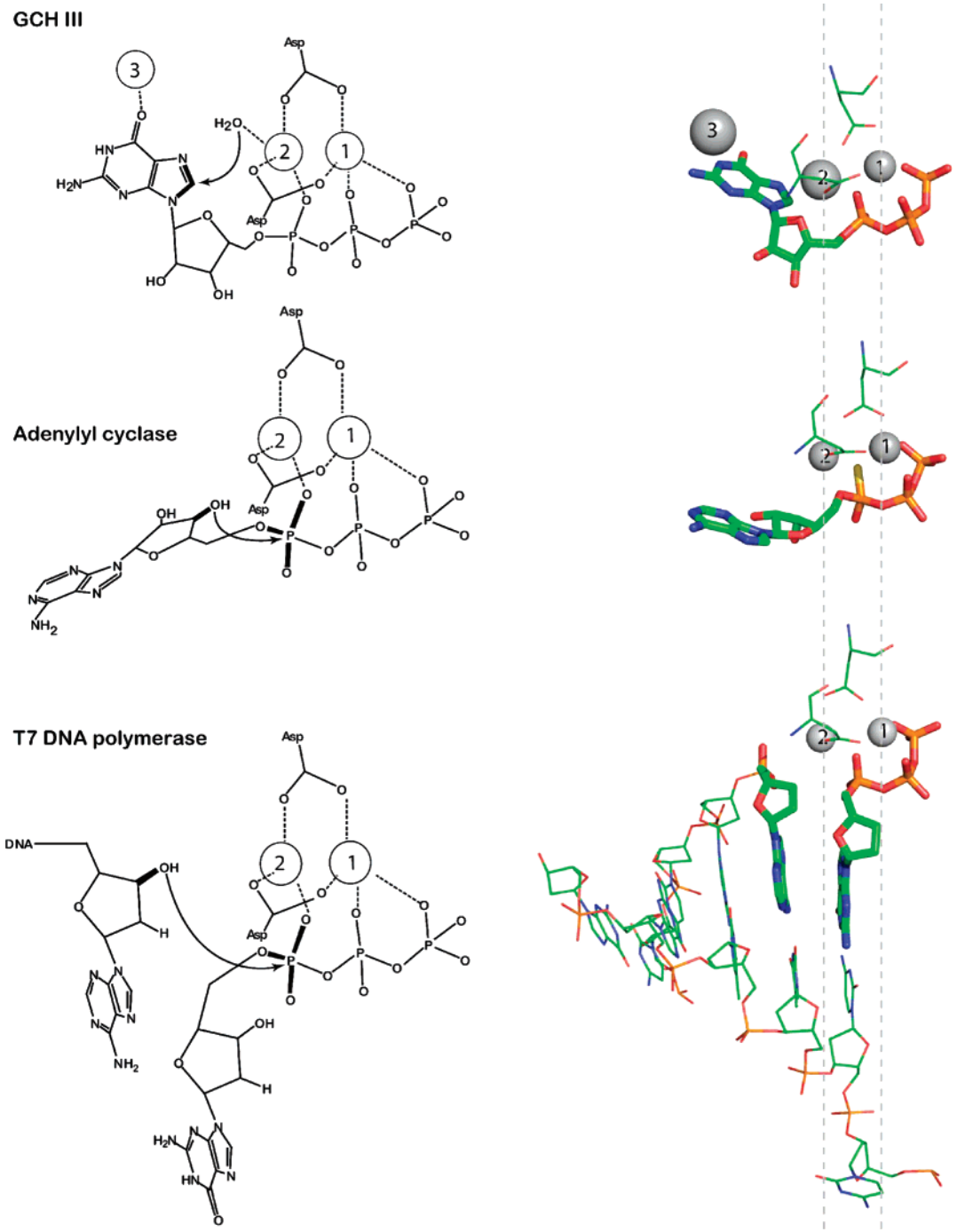

FIGURE 8: Comparison of two-metal ion sites of representative palm domain containing proteins. The palm domains of T7 DNA polymerase (1T7P), adenylyl cyclase (1CJK), and GCH III were superimposed to obtain the views that are shown. In each case, the substrate or substrate analog and the metal ions that were bound are shown. Although only T7 polymerase was solved in the presence of two Mg^{2+} ions, for simplicity, all of the metal ions are shown as gray. The dashed gray line denotes the positions of the metal ions in the structures.

presence. We believe that it is noteworthy that the presence of two metal ion binding sites, which resemble that in GCH III, are found in enzymes that catalyze phosphodiester cleavage reactions. Indeed, if GCH III shares common ancestry with other palm domain containing proteins, the primary reactions of which entail phosphodiester hydrolysis and *not* cyclohydrolase chemistry, the dephosphorylation that is observed in the course of conversion of GTP to FAPy may be rationalized as a promiscuous reactivity.

Consistent with the notion that the phosphodiester cleavage may represent a promiscuous side reaction, GCH III has been shown to catalyze the hydrolysis of inorganic pyrophosphate (*5*). Intriguingly, the reaction requires divalent metal ions; however, unlike in the conversion of GTP to FAPy, several metals that are unable to support conversion of GTP to FAPy function in the pyrophosphatase reaction. For instance, the pyrophosphatase activity of the protein in the presence of Co^{2+} was 45% that observed with Mg^{2+}; by contrast, the conversion of GTP to FAPy occurred at 0.6% of the rate with Mg^{2+} under similar conditions.

One may never know the ancestral role of palm domains in nature; however, palm-like domains are widely distributed in all kingdoms and are generally found in differing contexts. In bacteria, palm-like domains have been identified that are

fused to additional protein modules involved in signaling pathways (*36*). Since the common functional denominator in all proteins that contain these domains is phosphoryl transfer (with R-OH or water as acceptors), is it possible that the ancestral activity of this protein was dephosphorylation and that accretion or deletion of additional structural features, followed by evolution and selection, led to the diverse roles observed for these proteins in nature?

ACKNOWLEDGMENT

Portions of this research were carried out at the Stanford Synchrotron Radiation Laboratory, a national user facility operated by Stanford University on behalf of the U.S. Department of Energy, Office of Basic Energy Sciences. S.D.M. wishes to acknowledge James E. Spoonamore for help in HPLC analysis.

SUPPORTING INFORMATION AVAILABLE

A table that describes the anomalous data that was used to calculate the anomalous maps and confirm the metal assignments. This material is available free of charge via the Internet at http://pubs.acs.org.

REFERENCES

1. Burg, A. W., and Brown, G. M. (1968) The biosynthesis of folic acid. 8. Purification and properties of the enzyme that catalyzes the production of formate from carbon atom 8 of guanosine triphosphate. *J. Biol. Chem. 243*, 2349−2358.
2. Burg, A. W., and Brown, G. M. (1966) The biosynthesis of folic acid. VI. Enzymatic conversion of carbon atom 8 of guanosine triphosphate to formic acid. *Biochim. Biophys. Acta 117*, 275−278.
3. Foor, F., and Brown, G. M. (1975) Purification and properties of guanosine triphosphate cyclohydrolase II from *Escherichia coli*. *J. Biol. Chem. 250*, 3545−3551.
4. Foor, F., and Brown, G. M. (1980) GTP cyclohydrolase II from *Escherichia coli*. *Methods Enzymol. 66*, 303−307.
5. Graham, D. E., Xu, H., and White, R. H. (2002) A member of a new class of GTP cyclohydrolases produces formylaminopyrimidine nucleotide monophosphates. *Biochemistry 41*, 15074−15084.
6. Grochowski, L. L., Xu, H., Leung, K., and White, R. H. (2007) Characterization of an Fe(2+)-dependent archaeal-specific GTP cyclohydrolase, MptA, from *Methanocaldococcus jannaschii*. *Biochemistry 46*, 6658−6667.
7. Spoonamore, J. E., Dahlgran, A. L., Jacobsen, N. E., and Bandarian, V. (2006) Evolution of new function in the GTP cyclohydrolase II proteins of *Streptomyces coelicolor*. *Biochemistry 45*, 12144−12155.
8. Auerbach, G., Herrmann, A., Bracher, A., Bader, G., Gutlich, M., Fischer, M., Neukamm, M., Garrido-Franco, M., Richardson, J., Nar, H., Huber, R., and Bacher, A. (2000) Zinc plays a key role in human and bacterial GTP cyclohydrolase I. *Proc. Natl. Acad. Sci. U.S.A. 97*, 13567−13572.
9. Kaiser, J., Schramek, N., Eberhardt, S., Puttmer, S., Schuster, M., and Bacher, A. (2002) Biosynthesis of vitamin B2. An essential zinc ion at the catalytic site of GTP cyclohydrolase II. *Eur. J. Biochem. 269*, 5264−5270.
10. Kaiser, J., Schramek, N., Puttmer, S., Schuster, M., Eberhardt, S., Rebelo, J., Auerbach, G., Bader, G., Bracher, A., Nar, H., Hosl, C., Fischer, M., Huber, R., and Bacher, A. (2002) Essential zinc ions at the catalytic sites of GTP cyclohydrolases, in *Flavins and flavoproteins* (Chapman, S., Perham, R., and Scrutton, N., Eds.) pp 241−246, Rudolf Weber, Berlin.
11. Rebelo, J., Auerbach, G., Bader, G., Bracher, A., Nar, H., Hosl, C., Schramek, N., Kaiser, J., Bacher, A., Huber, R., and Fischer, M. (2003) Biosynthesis of pteridines. Reaction mechanism of GTP cyclohydrolase I. *J. Mol. Biol. 326*, 503−516.
12. Ren, J., Kotaka, M., Lockyer, M., Lamb, H. K., Hawkins, A. R., and Stammers, D. K. (2005) GTP cyclohydrolase II structure and mechanism. *J. Biol. Chem. 280*, 36912−36919.
13. Graham, D. E., R., O., Olsen, G. J., and Woese, C. R. (2000) An archaeal genomic signature. *Proc. Natl. Acad. Sci. U.S.A. 97*, 3304−3308.
14. Doublie, S. (1997) Preparation of selenomethionyl proteins for phase determination. *Methods Enzymol. 276*, 523−530.
15. de Korte, D., Haverkort, W. A., Roos, D., and van Gennip, A. H. (1985) Anion-exchange high performance liquid chromatography method for the quantitation of nucleotides in human blood cells. *Clin. Chim. Acta 148*, 185−196.
16. Pflugrath, J. W. (1999) The finer things in X-ray diffraction data collection. *Acta Crystallogr. D Biol. Crystallogr. 55*, 1718−1725.
17. Terwilliger, T. C. (2003) SOLVE and RESOLVE: Automated structure solution and density modification. *Methods Enzymol. 374*, 22−37.
18. Terwilliger, T. C. (2000) Maximum-likelihood density modification. *Acta Crystallogr. D Biol. Crystallogr. 56*, 965−972.
19. Cowtan, K. (2006) The Buccaneer software for automated model building. 1. Tracing protein chains. *Acta Crystallogr. D Biol. Crystallogr. 62*, 1002−1011.
20. McCoy, A. J., Grosse-Kunstleve, R. W., Storoni, L. C., and Read, R. J. (2005) Likelihood-enhanced fast translation functions. *Acta Crystallogr. D Biol. Crystallogr. 61*, 458−464.
21. Perrakis, A., Morris, R., and Lamzin, V. S. (1999) Automated protein model building combined with iterative structure refinement. *Nat. Struct. Biol. 6*, 458−463.
22. Emsley, P., and Cowtan, K. (2004) Coot: Model-building tools for molecular graphics. *Acta Crystallogr. D Biol. Crystallogr. 60*, 2126−2132.
23. Murshudov, G. N., Vagin, A. A., and Dodson, E. J. (1997) Refinement of macromolecular structures by the maximum-likelihood method. *Acta Crystallogr. D Biol. Crystallogr. 53*, 240−255.
24. DeLano, W. L. (2002) *The PyMol molecular graphics system*, DeLano Scientific, San Carlos, CA.
25. Collaborative Computational Project Number 4. (1994) The CCP4 suite: Programs for protein crystallography. *Acta Crystallogr. Sect. D 50*, 760−763.
26. Holm, L., and Sander, C. (1993) Protein structure comparison by alignment of distance matrices. *J. Mol. Biol. 233*, 123−138.
27. Tesmer, J. J. G., Sunahara, R. K., Gilman, A. G., and Sprang, S. R. (1997) Crystal structure of the catalytic domains of adenylyl cyclase in a complex with G_{Sa}•GTPgS. *Science 278*, 1907−1916.
28. Zhang, G., Liu, Y., Qin, J., Vo, B., Tang, W. J., Ruoho, A. E., and Hurley, J. H. (1997) Characterization and crystallization of a minimal catalytic core domain from mammalian type II adenylyl cyclase. *Protein Sci. 6*, 903−908.
29. Zhang, G., Liu, Y., Ruoho, A. E., and Hurley, J. H. (1997) Structure of the adenylyl cyclase catalytic core. *Nature 386*, 247−253.
30. Tesmer, J. J. G., Sunahara, R. K., Johnson, R. A., Gosselin, G., Gilman, A. G., and Sprang, S. R. (1999) Two-metal-ion catalysis in adenylyl cyclase. *Science 285*, 756−760.
31. Findeisen, F., Linder, J. U., Schultz, A., Schultz, J. E., Brugger, B., Wieland, F., Sinning, I., and Tews, I. (2007) The structure of the regulatory domain of the adenylyl cyclase Rv1264 from Mycobacterium tuberculosis with bound oleic acid. *J. Mol. Biol. 369*, 1282−1295.
32. Chan, C., Paul, R., Samoray, D., Amiot, N. C., Giese, B., Jenal, U., and Schirmer, T. (2004) Structural basis of activity and allosteric control of diguanylate cyclase. *Proc. Natl. Acad. Sci. U.S.A. 101*, 17084−17089.
33. Ollis, D. L., Kline, C., and Steitz, T. A. (1985) Domain of *E. coli* DNA polymerase I showing sequence homology to T7 DNA polymerase. *Nature 313*, 818−819.
34. Murzin, A. G. (1988) How far divergent evolution goes in proteins. *Curr. Opin. Struct. Biol. 8*, 380−387.
35. Artymiuk, P. J., Poirrette, A. R., Rice, D. W., and Willett, P. (1997) A polymerase I palm in adenylyl cyclase? *Nature 388*, 33−34.
36. Pei, J., and Grishin, N. V. (2001) GGDEF domain is homologous to adenylyl cyclase. *Proteins 42*, 210−216.
37. Doublie, S., Tabor, S., Long, A. M., Richardson, C. C., and Ellenberger, T. (1998) Crystal structure of a bacteriophage T7 DNA replication complex at 2.2 Å resolution. *Nature 391*, 251−258.
38. Steitz, T. A., and Steitz, J. A. (1993) A general two-metal-ion mechanism for catalytic RNA. *Proc. Natl. Acad. Sci. U.S.A. 90*, 6498−6502.

39. Tesmer, J. J. G., and Sprang, S. R. (1998) The structure, catalytic mechanism and regulation of adenylyl cyclase. *Curr. Opin. Struct. Biol. 8*, 713−719.
40. Hurley, J. H. (1998) The adenylyl and guanylyl cyclase superfamily. *Curr. Opin. Struct. Biol. 8*, 770−777.
41. Joyce, C. M., and Steitz, T. A. (1994) Function and structure relationships in DNA polymerases. *Annu. Rev. Biochem. 63*, 777−822.
42. Yang, W., Lee, J. Y., and Nowotny, M. (2006) Making and breaking nucleic acids: Two-Mg2+-ion catalysis and substrate specificity. *Mol. Cell 22*, 5−13.
43. Allen, F. H. (2002) The Cambridge Structural Database: A quarter of a million crystal structures and rising. *Acta Crystallogr. B* 380−388.
44. Pingoud, A., Fuxreiter, M., Pingoud, V., and Wende, W. (2005) Type II restriction endonucleases: Structure and mechanism. *Cell. Mol. Life Sci. 62*, 685−707.
45. Kim, E. E., and Wyckoff, H. W. (1991) Reaction mechanism of alkaline phosphatase based on crystal structures. Two-metal ion catalysis. *J. Mol. Biol. 218*, 2289−2295.
46. Stahley, M. R., and Strobel, S. A. (2005) Structural evidence for a two-metal-ion mechanism of group I intron splicing. *Science 309*, 1587−1590.
47. Bacher, A., Eisenreich, W., Kis, K., Landenstein, R., Richter, G., Scheuring, J., and Weinkauf, S. (1993) in *Bioorganic Chemistry Frontiers* (Dugas, H., and Schmidtchen, F. P., Eds.), pp 147−193, Springer-Verlag, Berlin.
48. Ollis, D. L., Brick, P., Hamlin, R., Xuong, N. G., and Steitz, T. A. (1985) Structure of large fragment of *Escherichia coli* DNA polymerase I complexed with dTMP. *Nature 313*, 762−766.
49. Artymiuk, P. J., Poirrette, A. R., Rice, D. W., and Willett, P. (1997) A polymerase I palm in adenylyl cyclase. *Nature 388*, 33−34.
50. O'Brien, P. J., and Herschlag, D. (1999) Catalytic promiscuity and the evolution of new enzymatic activities. *Chem. Biol. 6*, R91−R105.
51. Glasner, M. E., Gerlt, J. A., and Babbitt, P. C. (2006) Evolution of enzyme superfamilies. *Curr. Opin. Chem. Biol. 10*, 492−497.
52. Colloc'h, N., el Hajji, M., Bachet, B., L'Hermite, G., Schiltz, M., Prange, T., Castro, B., and Mornon, J. P. (1997) Crystal structure of the protein drug urate oxidase−inhibitor complex at 2.05 Å resolution. *Nat. Struct. Biol. 4*, 947−952.
53. Tanaka, Y., Nakagawa, N., Kuramitsu, S., Yokoyama, S., and Masui, R. (2005) Novel reaction mechanism of GTP cyclohydrolase I. High-resolution X-ray crystallography of *Thermus thermophilus* HB8 enzyme complexed with a transition state analogue, the 8-oxoguanine derivative. *J. Biochem. (Tokyo) 138*, 263−275.

BI701782E